17th World Conference on Earthquake Engineering, 17WCEE
Sendai, Japan - September 13th to 18th 2020

COMPARISON OF CONTACT MODELS FOR MOAT WALL POUNDING IN A BASE-ISOLATED MOMENT FRAME

P. J. Hughes[1], G. Mosqueda[2]

[1] *Graduate student researcher, University of California – San Diego, pjhughes@ucsd.edu*
[2] *Professor, University of California – San Diego,*
…

Abstract

Base isolation reduces seismic accelerations in buildings at the cost of increased displacements at the isolation plane. Under extreme shaking, the superstructure may displace beyond the provided clearance and collide with the surrounding moat wall. Most studies of this phenomenon employ "macro" elements that represent the moat wall with varying levels of detail, usually with a small number of springs and/or dashpots. The choice in contact model in these macro elements will invariably affect the predicted seismic response – a detail that has thus far been studied with simplified, often linear elastic, models of the superstructure and isolation system. This research examines how five different contact models affect the local impact behavior of a quarter-scale base-isolated moment frame, using a nonlinear structural model previously validated by experimental data – a unique feature of this study. Results indicate that the choice of contact model can moderately change the local impact dynamics. This effect is considerably higher for flexible moat walls with higher inherent damping.

Keywords: seismic isolation, moat wall, pounding ,contact

17th World Conference on Earthquake Engineering, 17WCEE
Sendai, Japan - September 13th to 18th 2020

1. Introduction

Base isolation is a proven seismic protection strategy that decreases floor accelerations at the cost of increased base displacements [1]. Under extreme ground motion, the base mat displacement may exceed the provided gap distance and impact the moat wall [2,3]. Moat wall pounding can induce very large accelerations and drift demands, diminishing the effectiveness of the isolation system [4–8].

Studies of moat wall pounding typically employ so-called macro models to represent the contact interface [2,5,9–12]. This means that contact between the superstructure and moat wall is defined using relatively simple uniaxial springs. As a result, analysts working on seismic pounding problems can choose from a wide range of contact models [13–20].

Several researchers [9,11,13,16] have assessed how different contact models affect the pounding response of isolated structures, but these studies are generally limited to single degree of freedom examples, or only consider a linear elastic superstructure. This research extends those studies to account for complexities in the superstructure and moat wall by using an OpenSees [21] model that has been calibrated to experimental pounding data [4,5]. More specifically, this work examines five specific contact models: linear elastic (E), linear viscoelastic (V) [13–15], Jankowski (J) [16,17], Hertzdamp (H) [18–20], and Muthukumar (M) [19].

2. Contact Model Overview

The contact models considered here relate the contact force f_c to a material-level indentation δ, and in some cases, the indentation velocity $\dot{\delta}$. Figure 1 shows the contact force-indentation hysteresis curves for every contact model. Tables 1 and 2 summarize the parameters and constitutive relationships of each contact model. For a detailed discussion of the parameters, the reader is directed to [13–20,22].

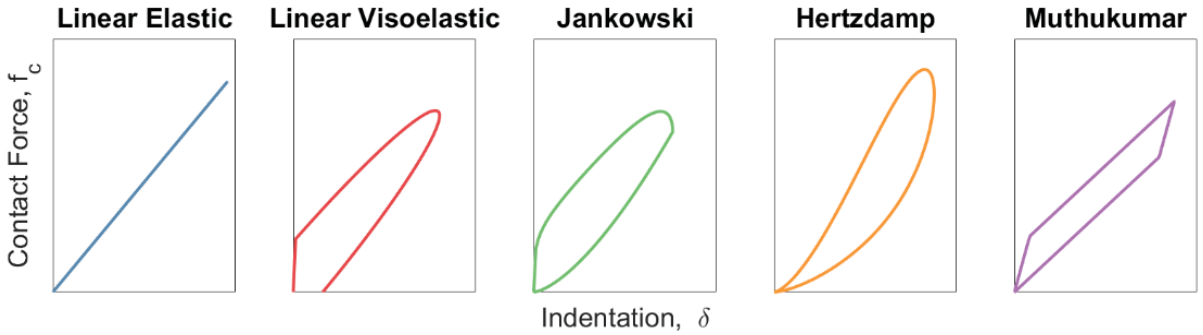

Fig. 1 – Contact force-indentation (f_c-δ) curves of every contact model.

17th World Conference on Earthquake Engineering, 17WCEE
Sendai, Japan - September 13th to 18th 2020

Table 1 – Contact model parameters.

Parameter Type	Symbol	Meaning	Units	Used in Models
Forces	f_m	maximum contact force	force	M
Deformations	δ_y	yield indentation	length	M
	δ_{me}	maximum expected indentation	length	E, V, M
	δ_m	maximum indentation	length	M
	$\dot{\delta}_0$	pre-impact indentation velocity	length/time	H
Stiffnesses	k_h	Hertz stiffness	force/length$^{3/2}$	E, V, J, H, M
	k_{eff}	effective linear stiffness	force/length	E, V, M
	k_1, k_2	initial, secondary stiffness	force/length	M
Damping Coefficients/Ratios	c_{eff}	effective linear damping coefficient	mass/time	V
	c_J	Jankowski damping coefficient	mass/time	J
	c_h	Hertz damping coefficient	mass/time	H
	ξ_{KV}	Kelvin-Voigt damping ratio	-	V
	ξ_J	Jankowski damping ratio	-	J
	ξ_h	Hertz damping ratio	-	H
Other	m_{eff}	effective mass	mass	V, J
	e	coefficient of restitution	-	V, J, H, M
	a	yield indentation ratio	-	M

Table 2 – Contact model constitutive laws.

Model Name	Constitutive Law	Input Parameters
Linear Elastic	$f_c=k_{eff}\delta$	$k_{eff}=k_h\sqrt{\delta_{me}}$
Linear Viscoelastic [13–15]	$f_c=k_{eff}\delta+c_{eff}\dot{\delta}$	$k_{eff}=k_h\sqrt{\delta_{me}}$ $c_{eff}=2\xi_{KV}\sqrt{m_{eff}k_{eff}}$ $\ln\left(\frac{1}{e}\right)=\frac{2\xi_{KV}}{\sqrt{1-\xi_{KV}^2}}\arctan\left(\frac{\sqrt{1-\xi_{KV}^2}}{\xi_{KV}}\right)$
Jankowski [16,17]	$f_c=\begin{cases}k_h\delta^{3/2}+c_J\dot{\delta} & , \dot{\delta}>0\\ k_h\delta^{3/2} & , \dot{\delta}\le 0\end{cases}$	k_h $c_J=2\xi_J\sqrt{m_{eff}k_h\sqrt{\delta}}$ $\xi_J=\frac{9\sqrt{5}}{2}\cdot\frac{1-e^2}{e(e(9\pi-16)+16)}$
Hertzdamp [18–20]	$f_c=k_h\delta^{3/2}+c_h\dot{\delta}$	k_h $c_h=\xi_h\frac{k_h}{\dot{\delta}_0}\delta^{3/2}$ $\xi_h=\frac{8}{5}\cdot\frac{1-e}{e}$
Muthukumar [19]	$f_c=\begin{cases}k_1\delta & , \dot{\delta}>0 \text{ and } \delta\le\delta_y\\ k_1\delta_y+k_2[\delta-\delta_y] & , \dot{\delta}>0 \text{ and } \delta>\delta_y\\ f_m-k_1[\delta_m-\delta] & , \dot{\delta}\le 0 \text{ and } \delta_m-\delta_y<\delta\le\delta_m\\ f_m-k_1(\delta_m-\delta_y)-k_2[\delta_m-\delta_y-\delta] & , \dot{\delta}\le 0 \text{ and } \delta<\delta_m-\delta_y\end{cases}$	$k_1=\left(1+\frac{2}{5}\cdot\frac{1-e^2}{a}\right)k_{eff}$ $\delta_y=a\delta_{me}$ $k_2=\left(1-\frac{2}{5}\cdot\frac{1-e^2}{1-a}\right)k_{eff}$ $0<a<1$

3. OpenSees Model

The contact models are implemented into a nonlinear OpenSees model, which has been previously calibrated to the experimentation described in [4]. This model employs the Masroor impact element [5], shown in Figure 2. This element is described by two systems in series: (1) a Muthukumar contact spring that represents the material indentation, and (2) a single degree-of-freedom (SDOF) system that represents the moat wall's global deformation.

All five contact models considered here share a common set of parameters (k_{eff}, m_{eff}, δ_{me}, and e). Furthermore, the vibrational part of the Masroor impact element has three parameters of its own: the 1st modal stiffness (K_1), 1st modal mass (M_1), and the impact damping ratio (C_{imp}). All values for the contact and vibrational components of the Masroor impact element are summarized in Table 3. This study considers two types of moat wall (concrete and steel), so there are two parameter sets listed. For both concrete and steel moat walls, the maximum expected indentation is set to 0.025″, and the yield indentation ratio (a) is set to 0.1, per the recommendations in [19]. The coefficient of restitution is 0.7 for both walls, a nominal value for civil engineering materials subject to low-velocity impacts [23].

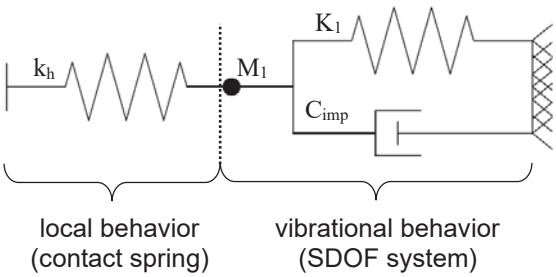

Fig. 2 – Masroor impact element.

Table 3 – Common parameters used in the Masroor impact element.

Spring Type	Parameter	Symbol	Moat Wall Type		Units
			Concrete	Steel	
Contact Spring	Hertz stiffness	k_h	6,700	11,000	kip/in$^{3/2}$
	Effective weight	$m_{eff} \cdot g$	0.29	0.40	kip
	Maximum expected indentation	δ_{me}	0.025	0.025	in
	Coefficient of restitution	e	0.70	0.70	-
	Yield indentation ratio	a	0.10	0.10	-
Vibration Spring	1st modal stiffness	K_1	2.4	100	kip/in
	1st modal weight	$M_1 \cdot g$	0.29	0.41	kip
	Impact damping ratio	ξ_{imp}	200	40	%
	Impact damping coefficient	C_{imp}	3.3	5.1	kip-sec/in

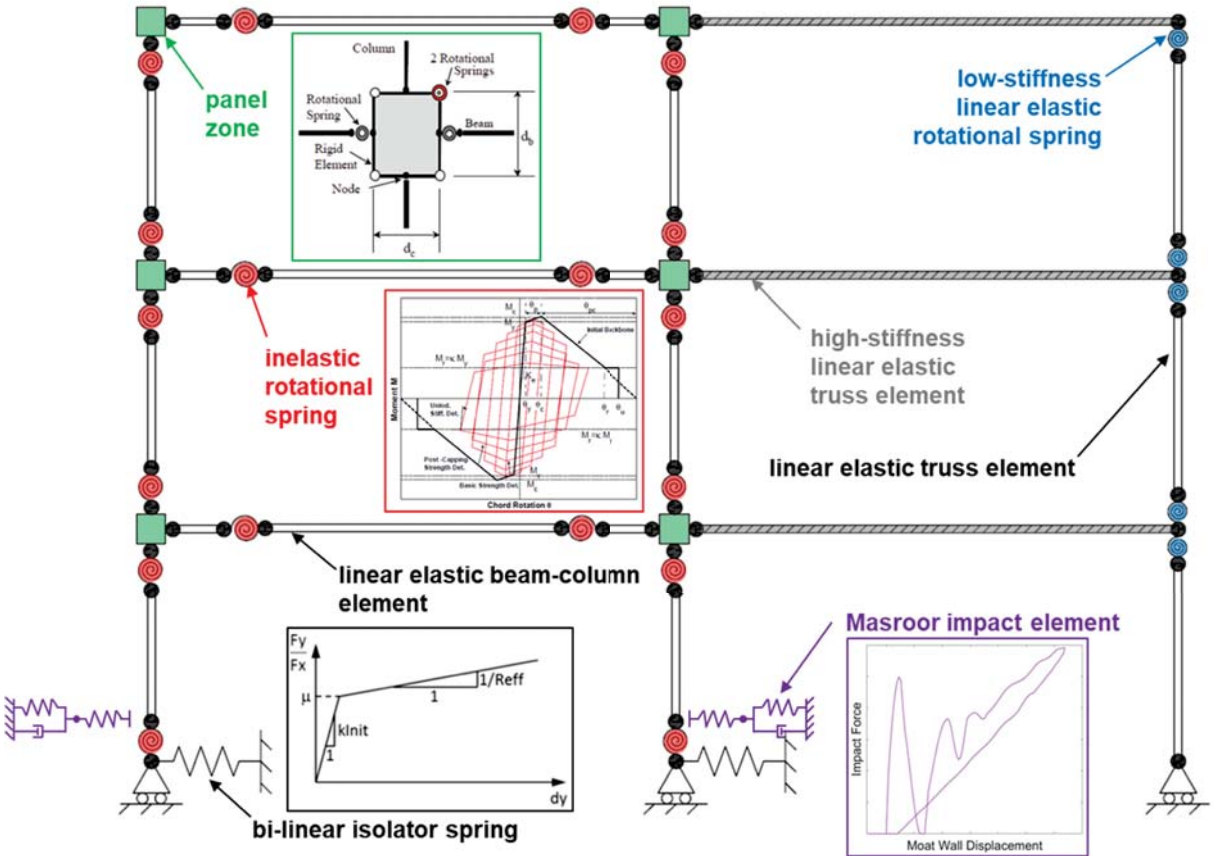

Fig. 3 – Schematic of the calibrated OpenSees model.

Other aspects of the OpenSees model are explained in detail in [7], but is summarized here for clarity. Panel zones [24] with the modified Ibarra-Krawinkler deterioration model [25,26] (Bilin material command) are used to model yielding of the superstructure. The SingleFPBearing element command is used to model the isolators. Figure 3 shows a diagram of the entire OpenSees model.

4. Contact Model Performance

The N-S component of the 1992 Erzincan earthquake, scaled to a peak ground acceleration (PGA) of 0.91 g, was the only impact-inducing ground motion used in the previous experimentation [4]. This motion is shown in Figure 4.

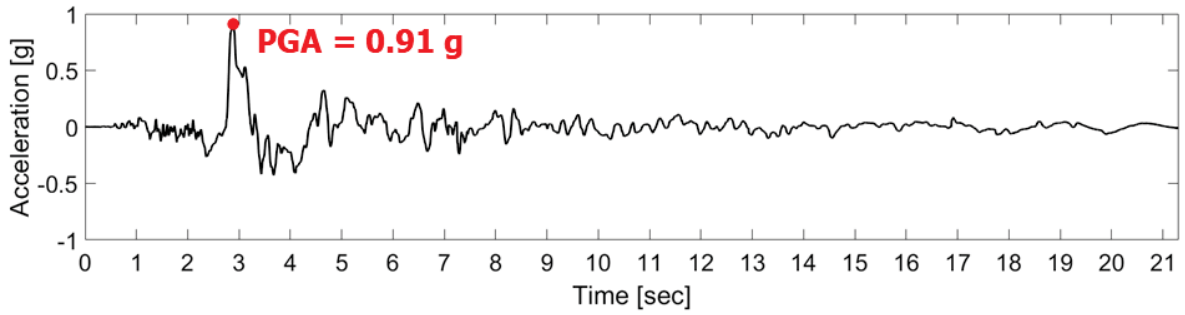

Fig. 4 – Impact-inducing ground motion (Erzincan 1992, N-S).

This acceleration record was used as a base excitation pattern in OpenSees, with two different moat wall materials (concrete, steel) and five different contact models. The gap distance is set to 4″ to match the experimental setup. Nonlinear dynamic time history results are summarized in Figures 5 – 7.

The impact force time histories are shown in Figure 5. For both wall materials, the difference between contact models is most noticeable in the early part of the contact duration, when the vibrational spring is not yet activated. Also, the linear elastic model exhibits high-amplitude oscillations relative to other contact models, particularly in the steel wall. This is because the linear elastic model has neither viscous nor hysteretic damping associated with it.

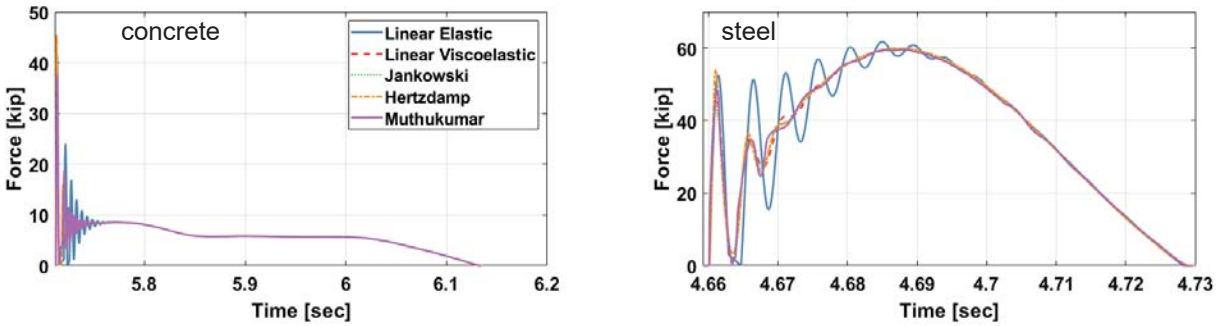

Fig. 5 – Impact force time histories.

Figure 6 emphasizes an expected difference between the contact models – the local hysteresis of the contact spring. All models show the same basic shapes seen in Figure 1, but with more oscillations caused by the higher-mode frequencies of the OpenSees model. While the shape of each hysteresis curve is obviously different, peak force and peak indentation are comparable for all cases.

In contrast to the local hysteresis curves, the global hysteresis curves in Figure 7 show subtler differences between the contact models. This is because the Masroor element can be viewed as two springs in series, where the more flexible spring (i.e. the vibrational spring) dominates.

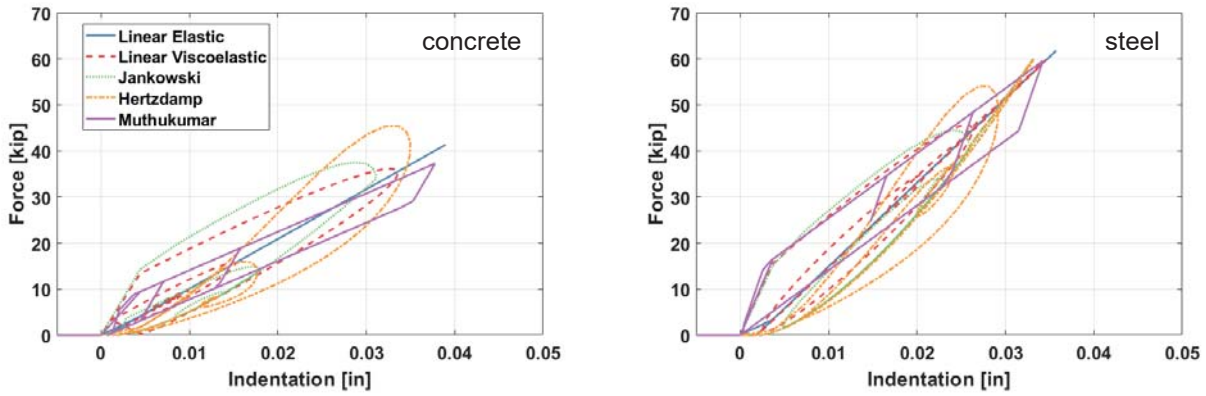

Fig. 6 – Contact spring hysteresis.

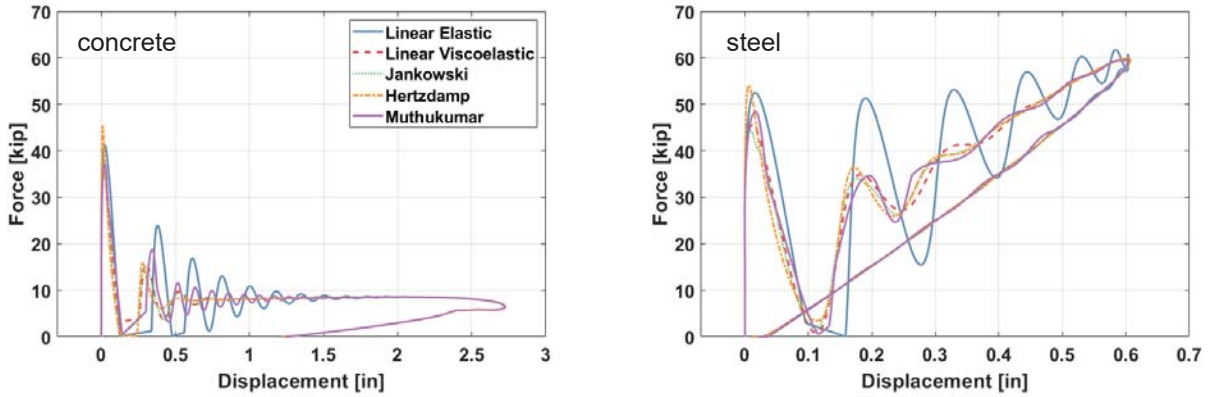

Fig. 7 – Vibrational spring hysteresis.

5. Conclusions

This research reviews several state-of-the-art contact models: linear elastic, linear viscoelastic, Jankowski, Hertzdamp, and Muthukumar. Each contact model is implemented into a nonlinear finite element model, previously calibrated to experimental moat wall pounding data. All contact models have similar impact force time histories for the single ground motion considered here. This is because impact between the base mat and moat wall initiates at the contact spring, where the differences between contact models is most significant. Later in the contact duration, the contact spring is fully compressed, and the vibrational spring dominates. This can also be seen in the global hysteresis of the moat wall, where differences between the contact models vanishes at or before the point of peak wall displacement. All models show roughly the same peak impact force and peak wall displacement.

This study shows preliminary findings of a much larger work in progress. Future work will examine how each contact model affects global response features of the entire building, such as floor acceleration and interstory drift ratio. It is also important to investigate how the conclusions of this paper would vary when applied to a wider suite of ground motions, particularly for near-fault earthquakes, where moat wall pounding is most likely to occur. Other variables, such as superstructure type (braced frame, shear wall, etc.) will also be studied.

6. References

[1] C. Christopoulos, A. Filiatrault, Principles of Passive Supplemental Damping and Seismic Isolation, IUSS Press. (2006).

[2] S. Nagarajaiah, X. Sun, T.L. Angeles, C. Fire, B.F.C.C. Building, Base-Isolated FCC Building: Impact Response in Northridge Earthquake, J. Struct. Eng. 127 (2001) 1063–1075. https://doi.org/10.1061/(ASCE)0733-9445(2001)127:9(1063).

[3] H.P. Gavin, R.L. Nigbor, Performance of the base-isolated Christchurch women's hospital in the Sep. 4 2010 Dar field earthquake and the Feb.22 2011 Christchurch earthquake, 20th Anal. Comput. Spec. Conf. - Proc. Conf. (2012) 554–563. https://doi.org/10.1061/9780784412374.049.

[4] A. Masroor, G. Mosqueda, Experimental simulation of base-isolated buildings pounding against moat wall and effects on superstructure response, Earthq. Eng. Struct. Dyn. (2012). https://doi.org/10.1002/eqe.2177.

[5] A. Masroor, G. Mosqueda, Impact model for simulation of base isolated buildings impacting flexible moat walls, Earthq. Eng. Struct. Dyn. (2013). https://doi.org/10.1002/eqe.2210.

[6] A. Masroor, G. Mosqueda, Assessing the collapse probability of base-isolated buildings considering pounding to moat walls using the FEMA P695 methodology, Earthq. Spectra. 31 (2015) 2069–2086. https://doi.org/10.1193/092113EQS256M.

[7] A. Masroor, G. Mosqueda, Seismic response of base isolated buildings considering pounding to moat walls, 2013.

[8] T. Sasaki, E. Sato, K. Fukuyama, K. Kajiwara, Enhancement of Base-Isolation Based on E-Defense Full-Scale Shake Table Experiments : Dynamic Response of Base- Isolated Building Under Impact Due To Pounding, 4082 (2017).

[9] H.C. Tsai, Dynamic analysis of base-isolated shear beams bumping against stops, Earthq. Eng. Struct. Dyn. 26 (1997) 515–528. https://doi.org/10.1002/(SICI)1096-9845(199705)26:5<515::AID-EQE654>3.0.CO;2-C.

[10] P.K. Malhotra, Dynamics of seismic impacts in base-isolated buildings, Earthq. Eng. Struct. Dyn. 26 (1997) 797–813. https://doi.org/10.1002/(sici)1096-9845(199708)26:8<797::aid-eqe677>3.3.co;2-y.

[11] P. Komodromos, P.C. Polycarpou, L. Papaloizou, M.C. Phocas, Response of seismically isolated buildings considering poundings, Earthq. Eng. Struct. Dyn. (2007). https://doi.org/10.1002/eqe.692.

[12] A. Sarebanha, G. Mosqueda, M.K. Kim, J.H. Kim, Seismic response of base isolated nuclear power plants considering impact to moat walls, Nucl. Eng. Des. 328 (2018) 58–72. https://doi.org/10.1016/j.nucengdes.2017.12.021.

[13] S. Goyal, E.N. Pinson, F.W. Sinden, Simulation of dynamics of interacting rigid bodies including friction I: General problem and contact model, Eng. Comput. (1994). https://doi.org/10.1007/BF01198742.

[14] S. Goyal, E.N. Pinson, F.W. Sinden, Simulation of dynamics of interacting rigid bodies including friction II: Software system design and implementation, Eng. Comput. (1994). https://doi.org/10.1007/BF01198743.

[15] B. Brogliato, Nonsmooth mechanics: Models, dynamics and control, Third edition, in: Commun. Control Eng., 2016. https://doi.org/10.1007/978-3-319-28664-8.

[16] R. Jankowski, Non-linear viscoelastic modelling of earthquake-induced structural pounding, Earthq. Eng. Struct. Dyn. 34 (2005) 595–611. https://doi.org/10.1002/eqe.434.

[17] R. Jankowski, Analytical expression between the impact damping ratio and the coefficient of restitution in the non-linear viscoelastic model of structural pounding, Earthq. Eng. Struct. Dyn. 35 (2006) 517–524. https://doi.org/10.1002/eqe.537.

[18] H.M. Lankarani, P.E. Nikravesh, A contact force model with hysteresis damping for impact analysis of multibody systems, J. Mech. Des. Trans. ASME. 112 (1990) 369–376. https://doi.org/10.1115/1.2912617.

[19] S. Muthukumar, R. DesRoches, A Hertz contact model with non-linear damping for pounding simulation, Earthq. Eng. Struct. Dyn. 35 (2006) 811–828. https://doi.org/10.1002/eqe.557.

[20] K. Ye, L. Li, H. Zhu, A note on the Hertz contact model with nonlinear damping for pounding simulation, (2009) 1135–1142. https://doi.org/10.1002/eqe.

[21] F. McKenna, G.L. Fenves, M.H. Scott, Open system for earthquake engineering simulation, University of California, Berkeley, 2000.

[22] W. Goldsmith, J.T. Frasier, Impact: The Theory and Physical Behavior of Colliding Solids, J. Appl. Mech. (1961). https://doi.org/10.1115/1.3641808.

[23] R. Jankowski, Experimental study on earthquake-induced pounding between structural elements made of different building materials, Earthq. Eng. Struct. Dyn. (2010). https://doi.org/10.1002/eqe.941.

[24] A. Gupta, H. Krawinkler, Seismic Demands for Performance Evaluation of Steel Moment Resisting Frame Structures, 1999.

[25] L.F. Ibarra, H. Krawinkler, Global Collapse of Frame Structures under Seismic Excitations, 2005.

[26] D.G. Lignos, H. Krawinkler, Deterioration modeling of steel components in support of collapse prediction of steel moment frames under earthquake loading, J. Struct. Eng. (2011). https://doi.org/10.1061/(ASCE)ST.1943-541X.0000376.

